Carbon Trends 13 (2023) 100302

Contents lists available at ScienceDirect

Carbon Trends

journal homepage: www.elsevier.com/locate/cartre

Synthesis, magnetoresistance, and thermoelectrical properties of environmentally stable n-type nitrogen-doped multiwalled carbon nanotubes

Jana Andzane [a], Mikhail V. Katkov [c], Krisjanis Buks [c], Anatolijs Sarakovskis [d], Krisjanis Smits [d], Donats Erts [a,b,*]

[a] Institute of Chemical Physics, University of Latvia, Raina blvd. 19, Riga, Latvia, LV-1586
[b] Faculty of Chemistry, University of Latvia, Raina blvd. 19, Riga, Latvia, LV-1586
[c] 3D Strong Ltd, Instituta str. 36–17, Ulbroka, Latvia, LV-2130
[d] Institute of Solid State Physics, University of Latvia, Kengaraga str. 8, Riga, Latvia, LV-1063

ARTICLE INFO

Keywords:
nitrogen-doped multiwalled carbon nanotubes
N-MWCNT
pyridine
Seebeck coefficient
annealing stability
low-temperature magnetoresistance

ABSTRACT

Nitrogen-doped multiwalled carbon nanotubes (N-MWCNTs) are known as a perspective material for a variety of applications in nanoelectronic devices, sensors, catalysts for carbon dioxide reduction, and flexible thermoelectrics. However, up to date most of the reports on the properties of N-MWCNTs are focused on a narrow niche of research, for example, a study of low-temperature magnetoresistance or room-temperature thermoelectrical properties. In this work, N-MWCNTs were synthesized using benzene:pyridine precursor in different ratios, and both magnetoresistance and thermoelectrical properties of the synthesized N-MWCNTs were systematically investigated in the temperature range 2-300 K and compared with the properties of undoped MWCNTs. Unexpected switching of the magnetoresistance of the N-MWCNTs at low temperatures from negative to positive values was observed, and the processes underlying this effect are discussed. The study of the thermoelectrical properties revealed n-type conductance in the N-MWCNTs, which was attributed to the impact of nitrogen defects incorporated in the MWCNT structure. Performed for the first-time investigations of the thermal stability of the Seebeck coefficient of N-MWCNTs in air revealed that the Seebeck coefficient retains its negative values and even increases after annealing of the N-MWCNTs in air at 500 °C. These findings illustrate the high potential of the presented in this work N-MWCNTs for applications in different devices in a wide range of temperatures.

1. Introduction

Multiwalled carbon nanotubes (MWCNTs) represent one of the most unique materials in the field of nanotechnology due to their great potential in different fields such as, for example, supercapacitors and batteries, sensors, electronic devices, gas and hydrogen storage, carbon dioxide reduction, and flexible thermoelectric composites [1]. A network of carbon nanotubes creates good electrical but not thermally conductive connections. That makes them favorable for thermoelectric applications of flexible devices as bare material [2,3] or in combination with conventional nanostructured inorganic thermoelectric materials [4–7]. For example, efficient flexible thermoelectric heterostructures can be prepared by direct physical vapor deposition of bismuth and antimony chalcogenides on MWCNT networks (CNT-TE heterostructures) [4]. However, naturally as-grown MWCNTs exhibit p-type conductance due to adsorbed from the environment oxygen [8]. Recently, our group showed that highly effective n-type MWCNT-Bi_2Se_3 heterostructures may be synthesized by physical vapour deposition of Bi_2Se_3 nanostructures directly on the network prepared from as-grown undoped p-type MWCNTs [4]. However, due to the competing conductance mechanisms of as-grown p-type MWCNTs and n-type Bi_2Se_3, the Seebeck coefficient of the resulting MWCNT-Bi_2Se_3 heterostructures is very sensitive to the concentration of MWCNTs and rapidly decreases with its increase [4]. Thus, the fabrication of CNT-TE heterostructures having n-type conductivity requires pre-treatment of the as-grown CNTs to convert their p-type conductance to n-type, which typically can be achieved by annealing of the as-grown CNTs under high vacuum to degass the adsorbed oxygen [9,10]. A significant drawback of this

* Corresponding author.
E-mail address: donats.erts@lu.lv (D. Erts).

https://doi.org/10.1016/j.cartre.2023.100302
Received 20 July 2023; Received in revised form 3 October 2023; Accepted 3 October 2023
Available online 5 October 2023

approach is that the fabricated heterostructure should be kept and used in high-purity inert atmosphere because under ambient conditions the conductivity type of the annealed CNTs transits from n- to p- within days [10,11], which may result in the degradation of n-type thermoelectric properties of the heterostructure.

An alternative way of obtaining MWCNT with a stable n-type is doping with boron or nitrogen during the synthesis [12–14]. MWCNTs may be synthesized by a variety of methods as classical or aerosol-assisted chemical vapor deposition (CVD) [15,16] laser ablation [17], supercritical fluid [18], and others. Among these methods, the aerosol-assisted CVD or pyrolysis has proven itself to be easily-reproducible and useful for the introduction of a significant proportion of nitrogen in the MWCNT structure [19]. To form nitrogen-containing carbon nanotubes under aerosol-assisted CVD conditions, additives of nitrogen-containing compounds such as acetonitrile [20,21], melamine [10,22], ammonia [12], and pyridine [23–25] can be used. As it is known, doped nitrogen atoms in the N-MWCNTs mainly exist in three forms: substitutional (graphite-like, graphitic), where the nitrogen atom replaces a graphitic carbon atom, pyridinic (pyridine--like) nitrogen, where the nitrogen atom is two-fold coordinated, and pyrrolic (pyrrole-like) nitrogen, where substitutional atom sits in five-fold ring [19]. Pyrrolic nitrogen is sp^3 coordinated, while pyridinic and graphitic nitrogen are both sp^2 coordinated. Pyridinic and pyrrole-like nitrogen are non-doping, whereas graphitic nitrogen generates a donor state. While the synthesis temperature is one of the determining factors for the proportions of these defects due to their different stability, some of the reports claim that at the same synthesis temperature, the precursor used may play a significant role in the resulting types and amounts of defects in the N-MWCNTs [21].

Between these nitrogen sources, the first two – acetonitrile and melamine – are the most widely used, while there is a very limited number of reports showing the use of pyridine for the synthesis of N-MWCNTs, and these reports are limited to the description of structure and morphology of the produced N-MWCNTs, but do not contain information on their properties.

In terms of properties, the research of N-MWCNTs is mostly focused on specific applications of N-MWCNT, for example, resistivity and magnetoresistance at low temperatures for electronic applications [20,26]; thermoelectrical properties for application in energy harvesting [10,14]; catalytic properties for carbon dioxide reduction [27]. However, to the best of our knowledge, there is no or very limited number of reports presenting investigation of different properties of the same batch of N-MWCNTs synthesized by any method. In addition, up to date very limited attention was paid to the investigation of thermal durability of N-MWCNTs at elevated temperatures in ambient air, which is crucial for the applications of N-MWCNT in thermoelectrics. To the best of our knowledge, the investigation of the durability of N-MWCNTs after annealing in air up to 300 °C was studied for the nanotubes synthesized using melamine as a nitrogen source and argon/acetylene as carrier gas and carbon source, however, this study was focused solely on the investigation of chemical composition and morphology of the N-MWCNTs.

In this work, N-MWCNTs were synthesized via spray-assisted CVD using as precursors benzene:pyridine (BZ:PY) mixture in different ratios, and a systematic study of electrical, magnetoresistance, and thermoelectrical properties of the synthesized using such precursors N-MWCNTs was performed for the first time. The properties of the N-MWCNTs were analyzed and compared with the properties of undoped MWCNTs, as well as with the reported properties of N-MWCNTs synthesized using different precursors.

2. Materials and methods

2.1. Synthesis of undoped MWCNTs and N-MWCNTs

The synthesis of nitrogen-doped multiwalled carbon nanotubes (N-MWCNT) was carried out by the spray-assisted chemical vapor deposition (CVD) method from a gas phase. The reactor vessel was made of a pyrolysis steel tube 2000 mm long and 100 mm in diameter, located inside a high-temperature tubular furnace. The quartz tube was placed inside the reactor vessel and sealed with stainless flanges equipped with the systems for the reaction mixture delivery and products removal. The synthesis of N-MWCNTs occurred in inert (argon) gas under atmospheric pressure at a flow rate of 20 mm·s^{-1}. The source of iron for the formation of catalytic particles was ferrocene dissolved in a mixture of benzene (BZ) and pyridine (PY) (1:3 and 1:19 by volume) for the synthesis of N-MWCNTs and in toluene for the synthesis of undoped MWCNTs. 100 ml of a mixture of BZ and PY with 2 wt.% of ferrocene was used for one synthesis cycle. The reaction mixture was delivered into the synthesis zone in the form of an aerosol by a dispenser. Spraying the mixture in the reactor was carried out in a zone with a temperature of about 200°C. The vapors of the reaction mixture were taken up by the carrier gas and transferred to the growth zone of carbon nanotube arrays. The synthesis was carried out for 20 min at a temperature of 850 °C for obtaining N-MWCNTs and for 60 min at a temperature 800 °C for obtaining undoped MWCNTs. At the end of the delivery of the reaction mixture, the reactor was purged with an argon flow for 20 min. This procedure is necessary to remove the residual reaction products. Then, the argon flow was stopped, and the reactor was shut off and cooled to room temperature. After cooling down, the reactor was disassembled, and the quartz tube was removed. The black film formed because of synthesis on the inner wall of the quartz tube and consisting of N-MWCNTs or undoped MWCNTs was removed mechanically.

2.2. Preparation of undoped MWCNT and N-MWCNT networks

Networks of undoped MWCNTs and N-MWCNTs were prepared on 10 mm × 5 mm and 10 mm × 10 mm glass substrates by spray-coating method. For the spray-coating, a 0.1 wt.% MWCNT or N-MWCNT-isopropyl alcohol (IPA) suspension was used to obtain carbon nanotube networks with different surface densities. During the spray-coating, the glass substrates were heated up to 120 °C to ensure fast evaporation of IPA thus preventing an unwanted agglomeration of CNTs.

Annealing of the samples was performed in air in a quartz tube furnace (GCL-1100x; MTI Corp.) for 40 mins at a temperature of 500 °C.

2.3. Structural characterization of the samples

The morphology and chemical composition of the synthesized carbon nanotubes were characterized using a Hitachi S-4800 field-emission scanning electron microscope equipped with the energy-dispersive X-ray diffraction analyzed (123 eV; Bruker XFlash Quad 5040). High-resolution images of the synthesized carbon nanotubes were obtained using transmission electron microscope FEI Technai GF 20. XPS analysis was performed using a ThermoFisher ESCALAB Xi+ instrument using an Al Kα monochromatic X-ray source. The instrument's binding energy counter was calibrated to give a binding energy of 932.6 eV for the Cu $2p_{3/2}$ line of freshly etched copper metal. The charge compensation system was used for all non-conductive specimens. The surface of each sample was irradiated with an electron beam to create an almost neutral surface charge. The spectra were recorded using a 900 × 10 μm X-ray beam with a transmission energy of 20 eV and a step size of 0.1 eV. The data for all materials were tied to the main signal of the carbon 1s spectrum, referred to the region of 285.0 eV. The carbon 1s spectrum was obtained using high-energy resolution settings. Fourier transform infrared spectra (FTIR) were measured with Bruker Vertex 70v, equipped with an attenuated total reflection module with diamond crystal. Spectral range 400-4000 cm^{-1}, resolution ±2 cm^{-1}, 20 spectra per measurement, 4 measurements per sample. The average spectrum was calculated and presented.

Magnetoresistance and thermoelectric measurements. Magnetoresistance (MR) is defined as MR=(ρ(B)-ρ(0))/(ρ(0)), where B is the

magnetic field strength, ρ(0) and ρ(B) are the MWCNT film resistivities in the presence and absence of magnetic field, respectively. For the magnetoresistance determination, the resistances of the MWCNT networks were measured in a classic Hall bar configuration using the physical property measurement system (PPMS DynaCool-9T, Quantum Design) at temperature and magnetic field strength in the range of 2 to 300 K and -9 T to +9 T, respectively. The samples were 10 mm x 10 mm in size; electrodes (70 nm Gold / 5 nm Titanium) were applied by the thermal evaporation method (SIDRABE SAF EM sputtering vacuum system). For the resistivity calculation, the thicknesses of the MWCNT networks were measured using profilometer Veeco Dektak 150.

The thermoelectric measurements in ambient conditions were performed in a two-point configuration using a laboratory-made device, consisting of Peltier modules, a programmable control block, and an HP34401A digital multimeter. The system was calibrated using Standard Reference Material 3451 for low-temperature Seebeck coefficient (NIST).

The thermoelectric measurements under high-vacuum conditions in the temperature range 10-300 K were performed in a 4-point configuration using a thermal transport option (TTO) of a physical property measurement system (PPMS) DynaCool-9T, Quantum Design. Sample size was 10 mm x 5 mm. Resistance and magnetoresistance measurements of the samples in the temperature range 2-300 K were performed using the resistivity option and electrical transport option of the PPMS (DynaCool-9T, Quantum Design).

3. Results and discussion

3.1. Structure of the N-MWCNTs

SEM images of the as-grown using pyridine as the nitrogen source N-MWCNTs revealed their arranged growth, forming densely packed arrays (Fig. 1 a), which is in line with the previously reported growth of N-CNT nanotubes via injection CVD method using ferrocene catalyst and pyrazine as the nitrogen source [28].

The outer diameters of the synthesized N-MWCNT varied from 30 to 100 nm, while the lengths of the nanotubes were in the range 50-100 μm. Comparison of the EDX spectra of the N-MWCNTs synthesized using BZ:PY ratio 1:19 with the undoped MWCNTs revealed the presence of a nitrogen-related peak in the spectrum of the N-MWCNT (Fig. 1 b, red curve), while the similar peak was absent in the EDX spectrum of undoped MWCNTs (Fig. 1 b, blue curve). The amount of presented in the N-MWCNTs nitrogen was 6 ± 2 at.%.

In addition, EDX spectra of undoped MWCNTs exhibited a significantly more intensive peak related to oxygen in comparison with the N-MWCNTs (5.5 ± 1 vs 2 ± 0.2 at.%, Fig. 1 b), which may indicate less effective adsorption of oxygen on the surfaces of N-MWCNTs due to the nitrogen doping, resulting in the change of dominating charge carrier type in the MWCNTs.

In addition, FTIR spectrum of the N-MWCNTs synthesized using BZ:PY ratio 1:19 revealed an observed broad absorption peak in the 1300-1600 cm^{-1} region (Fig. 1 c), which is expected to appear when the N atoms are bonded into the carbon network [29]. It should be noted that the distortion region around 1900-2400 cm^{-1} was caused by similar refraction indices of the analyzing material and the sample [30,31], and does not indicate show information about the chemical bonds in the sample.

TEM micrographs of the synthesized using pyridine as the nitrogen source N-MWCNTs revealed bamboo-like structure of the CNTs (Fig. 2 a-c), in which the inside of the tube is separated into a series of compartments.

The observed bamboo-like structure of the nitrogen-doped MWCNTs indicates the incorporation of pyridinic nitrogen atom defects in the structure of MWCNTs [23,25,32]. The outer walls of the N-MWCNTs are well-formed and ordered (Fig. 2 c, d).

This observation is in line with the previously reported structure of N-MWCNTs synthesized using BZ:PY precursors [24] and contradicts the reports on the structure of outer walls of N-MWCNTs synthesized using other nitrogen sources such as acetonitrile [33,34] or melamine [35], where significant distortion in the structure of outer walls of the N-MWCNTs was observed. Less pronounced distortion of the outer walls was observed for the N-MWCNTs synthesized using benzylamine [21]. Presumably, the level of distortion introduced in the walls of N-MWCNTs may be related to the bonding configurations of nitrogen source materials. While pyridine is represented by an aromatic ring, which has no side groups, and thus, may be easily embedded in the graphitic structure of the MWCNTs, the wall distortion in the N-MWCNTs synthesized using acetonitrile or melamine as nitrogen sources may be related to the side groups presented in the molecular structure of melamine and linear structure of acetonitrile molecules, complicating embedding in the structure of carbon nanotube walls.

XPS N 1s spectra confirmed the presence of all three – sp^2-coordinated pyridinic and graphitic, and sp^3-coordinated pyrrolic - forms of nitrogen in the N-MWCNTs synthesized using pyridine as the nitrogen source (Fig. 2 e, f). Deconvolution of the representative XPS spectra of the N-MWCNTs synthesized using BZ:PY ratio 1:3 (Fig. 2 e) and 1:19 (Fig. 2 f) revealed the presence of 3 components with N 1s electron binding energies of ~398.5 eV, ~399.9 eV, and ~401.1 eV.

The 398.5 eV peak (Fig. 2 e, f, yellow curve) can be assigned to nitrogen into a ring structure folding only two carbon atoms (edge position), i.e., pyridinic form [22]. The peak at 399.9 eV can be attributed to the pyrrolic nitrogen, i.e., three-fold coordinated nitrogen in a region of defective non-aromatic lattice [19,21]. Finally, the peak at 401.1 eV can be attributed to the graphite-like form of nitrogen that appears by

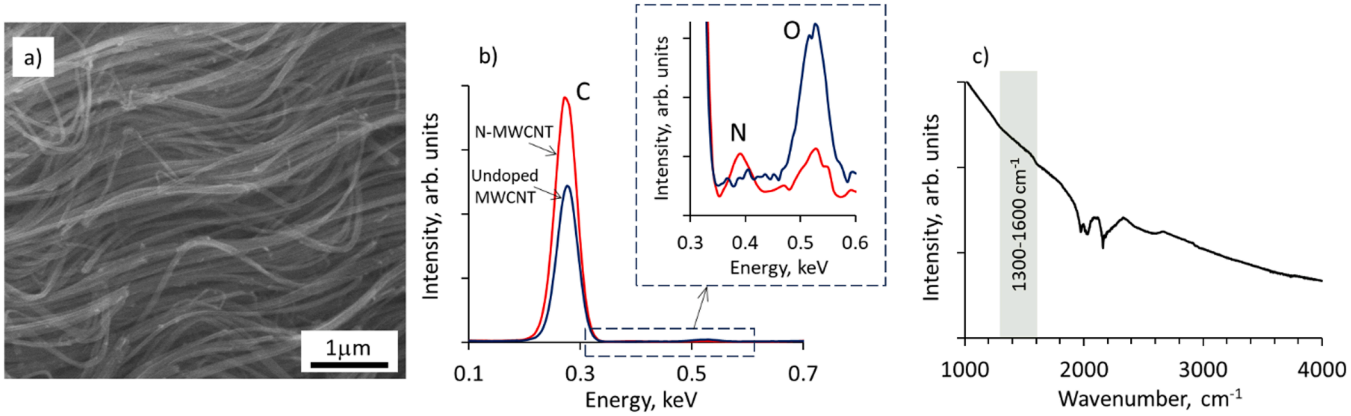

Figure 1. a) Scanning electron microscope (SEM) image of as-grown N-MWCNTs synthesized using BZ:PY ratio 1:19; b) comparison of the energy-dispersive X-ray diffraction (EDX) spectra of N-MWCNTs (red curve) and undoped MWCNTs (blue curve); c) Fourier transform Infrared (FTIR) spectrum of the N-MWCNTs.

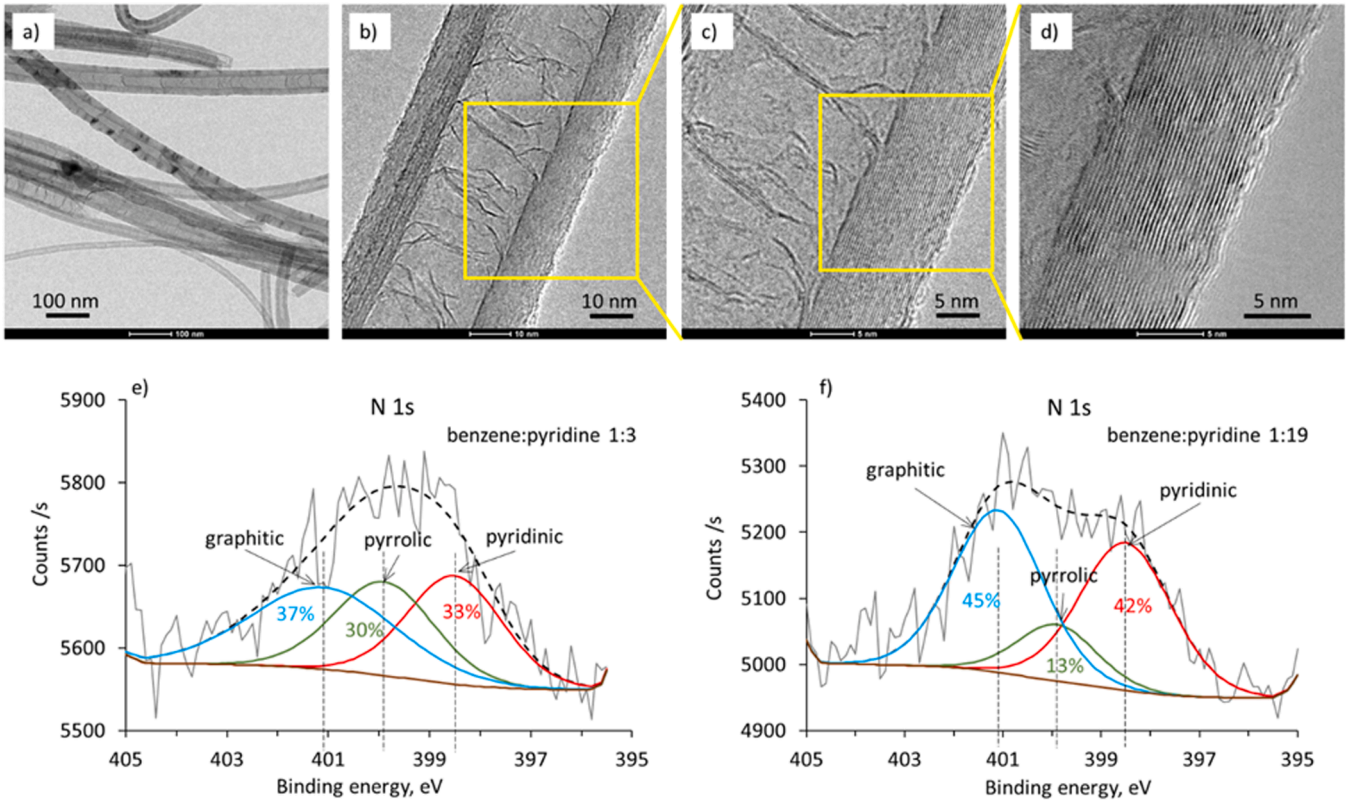

Figure 2. a-d) Transmission electron microscope (TEM) images of N-MWCNT structures: a) low-magnification image; b) higher-magnification image; c, d) close up views; e, f) X-ray photoelectron spectroscopy N 1s spectra of N-MWCNTs synthesized with benzene:pyridine (BZ:PY) ratio 1:3 (e) and 1:19 (f). The spectra are decomposed into components corresponding to graphitic, pyrrolic, and pyridinic nitrogen (in descending order of binding energy).

replacing a sp^2 carbon atom with a nitrogen one [22]. There were no peaks detected at ~405 eV, indicating that there is the absence or negligible amount of molecular nitrogen trapped inside the N-MWCNTs [32,36]. The total content of nitrogen in the N-MWCNTs determined from the XPS data was found to be ~0.8% and ~1.1% for the nanotubes synthesized using BZ:PY ratios 1:3 and 1:19 respectively (Table 1), which is similar to the total content of nitrogen detected by the XPS in the N-MWCNTs synthesized using acetonitrile with N/C ratios 1/135 (total N content in N-MWCNTs ~0.8%) and 1/9 (total content of N in N-MWCNTs ~1.2%), and significantly lower than N content detected in the N-MWCNTs synthesized using melamine as the nitrogen source (~7.6%, Table 1).

A significant difference between the nitrogen content detected in the N-MWCNTs by the EDX (~ 5.5 at.%) and by the XPS (~ 1.1 at.%) may be attributed to the difference in the measurement techniques: while the XPS technique allows analysis of the top few nanometers of the sample, the EDX is performed for ~ 1 μm deep volume of the sample, thus, the data obtained by the EDX may also reflect the nitrogen trapped in the inner volumes of the MWCNTs or physisorbed on their surfaces. Consequently, EDX and XPS techniques are complementary and qualitatively prove the incorporation of N in the MWCNTs, however, the data obtained by these techniques cannot be compared quantitatively. Further, the data obtained using the XPS technique will be analyzed as they provide additional information about the types of nitrogen defects in the MWCNTs.

Increasing the concentration of pyridine also changes the ratio between the different forms of nitrogen. As the concentration of nitrogen in the nanotubes increases, the amount of graphitic and pyridinic nitrogen increases from 37% and 33% at BZ:PY ratio 1:3 to 45% and 42% at BZ:PY ratio 1:19, respectively, while the amount of pyrrolic nitrogen decreases from 30% at BZ:PY ratio 1:3 to 13% BZ:PY ratio 1:19 (Fig. 2 f, Table 1).

Table 1
Proportions of nitrogen-related defects identified in N-MWCNTs, synthesized using different nitrogen sources (detected by XPS technique).

Nitrogen source	Total N content, %	Graphitic nitrogen, %	Pyridinic nitrogen, %	Pyrrolic nitrogen, %	Molecular nitrogen, %
Pyridine, this work BZ:PY ratio 1:3 N/C ratio 1/7	0.8	37	33	30	–
Pyridine, this work BZ:PY ratio 1:19 N/C ratio 1/5	1.1	45	42	13	–
Acetonitrile with toluene, N/C ratio 1/135 [21]	0.8	31	30	39	–
Acetonitrile with toluene, N/C ratio 1/9 [21]	1.2	51	28	21	–
Benzylamine, N/C ratio 1/7 [21]	1	65	27	8	–
Melamine [22]	7.6	42.7	35.1	14.1	1.2

The calculated from the peak areas' proportions of graphitic, pyrrolic and pyridinic nitrogen were respectively ~37%, ~30% and ~33% for the N-MWCNTs synthesized using BZ:PY ratio 1:3 (Fig. 2 e, Table 1) and ~45%, ~13% and ~42% for the N-MWCNTs synthesized using BZ:PY ratio 1:19 (Fig. 2 f, Table 1). In contrast with the sample synthesized using acetonitrile as the nitrogen source, which showed 39% and 21% of pyrrolic defects for the samples with N content of 0.8% and 1.2% respectively (Table 1), the samples synthesized using BZ:PY precursor showed lower proportion of pyrrolic nitrogen for the samples with the nitrogen content – 30% and 13% for the samples with N content of 0.8% and 1.1% respectively (Table 1). N-MWCNTs synthesized using BZ:PY ratio 1:3 showed also a higher by ~16.5% proportion of graphitic nitrogen defects in comparison with the similar sample synthesized using acetonitrile. Increase of N/C ratio in the BZ:PY precursor resulted in an increase of graphitic nitrogen in the N-MWCNTs by ~21% (Table 1), which is in line with the previously reported data for the N-MWCNTs synthesized using acetonitrile [21]. However, at the same time, N-MWCNTs synthesized using BZ:PY with the ratio 1:19 showed by ~50% higher proportion of pyridinic defects in comparison with the sample with similar nitrogen content, synthesized using acetonitrile (Table 1). Presumably, a higher proportion of pyridinic defects in N-MWCNTs synthesized using pyridine as the nitrogen source may be related to the molecular structure of pyridine, which is represented by an aromatic ring without side groups, thus allowing easier incorporation in the structure of MWCNTs.

3.2. *Electrical conductivity and magnetoresistance of undoped MWCNTs and N-MWCNTs*

The conductivity of N-MWCNTs with BZ:PY ratios 1:3 and 1:19 were respectively ~2 times and ~4.5 times lower compared to that of undoped MWCNTs (Fig. 3 a). This contradicts with the previous reports for the N-MWCNTs synthesized using acetonitrile as the source of nitrogen precursor, showing the increase in the conductivity of N-MWCNTs in comparison with the undoped MWCNTs due to the increase of the charge carrier number [20,37].

Temperature dependencies of conductivity of undoped MWCNTs (Fig. 3 a, grey dots) and N-MWCNTs, synthesized using BZ:PY ratios 1:3 (Fig. 3 a, red dots) and 1:19 (Fig. 2 a, blue dots) followed the logarithmic law $\sigma = a\ln T + b$, which is in line with the conductivity vs temperature dependencies reported for undoped [38] and nitrogen-doped using acetonitrile as a nitrogen source for the synthesis of N-MWCNT [20,37].

Logarithmic conductivity vs temperature dependencies are typically observed for disordered systems and nanocluster-assembled structures, exhibiting weak localization and/or electron-electron interaction effects [38,39]. According to the Efetov and Tshersich model [40], the slope of these curves is related to the average tunnelling conductance between neighboring clusters in the system as $a = \sigma_0/(\pi z G(e^2/\hbar))$, where σ_0 is conductivity at room temperature, G is the average tunnelling conductance between neighboring clusters, z is the coordination number (a number of neighbors for a single site on the array), and $(e^2/\hbar)$ is the quantum conductance. In turn, $G/(e^2/\hbar)$ is referred to as a dimensionless tunnelling conductance g_0.

Assuming that the coordination number z is the same for all samples,

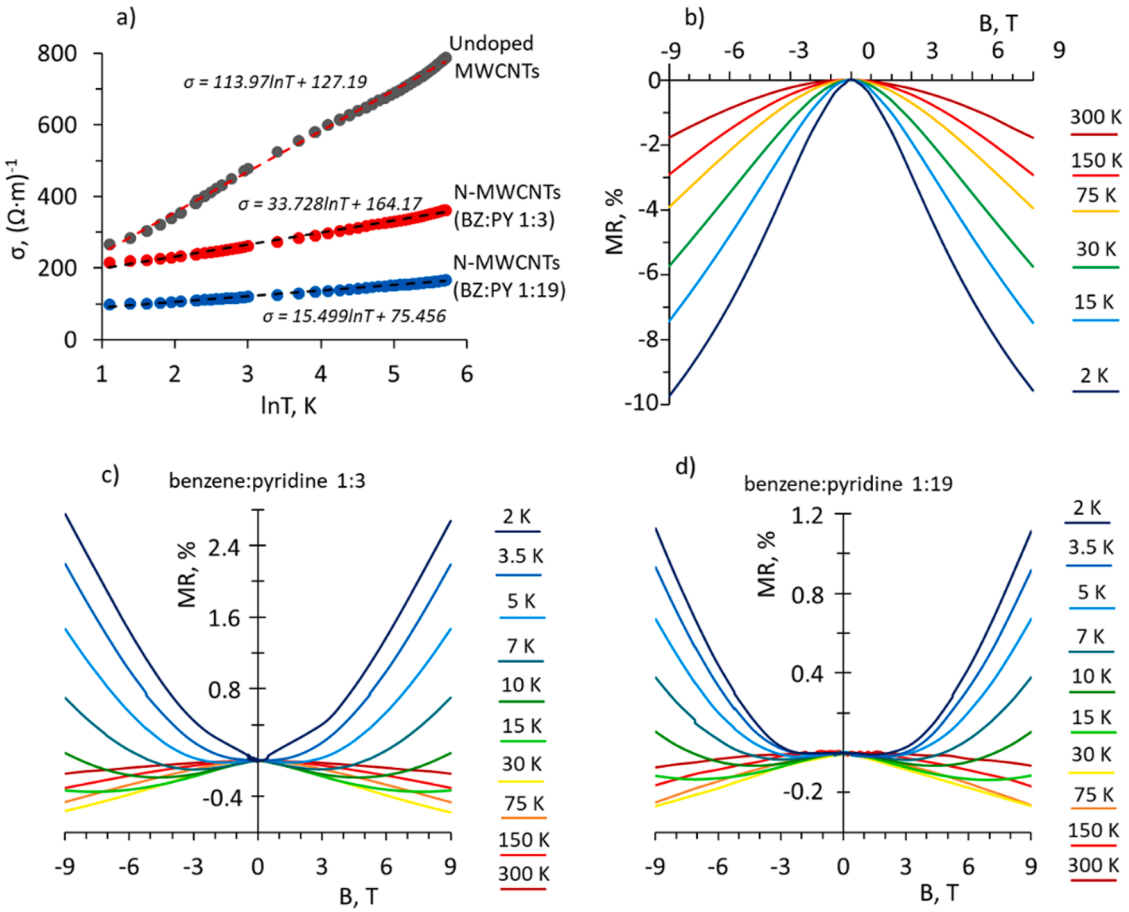

Figure 3. a) Conductivity vs temperature of undoped MWCNTs (grey dots) and N-MWCNTs synthesized using benzene:pyridine ratios 1:3 (red dots) and 1:19 (blue dots); b-d) Magnetoresistance as a function of magnetic field strength at different temperatures for samples of undoped MWCNTs (a), N-MWCNTs synthesized with the ratio of benzene and pyridine as 1:3 (b), and N-MWCNTs with the ratio of benzene and pyridine as 1:19 (c).

the relative comparison of g_0 showed that its value for the N-MWCNT networks synthesized using BZ:PY precursor is 3.427 and 3.431 for N-MWCNTs synthesized using BZ:PY concentrations 1:3 and 1:19 respectively, which is by ~1.55 times higher in comparison with g_0 value of 2.205 determined for undoped MWCNTs. Higher tunnelling conductance of N-MWCNT in comparison with undoped MWCNTS is in line with the previous reports, where the promotion of tunnelling current due to the impact of energy levels formed by N atoms, that deviate from the energy levels of sp^2 carbon has been reported. These results indirectly prove the incorporation of nitrogen in the structure of carbon.

Changes in the magnetoresistance of undoped MWCNTs networks (Fig. 3 b) are always negative in the full temperature range from 2 K up to 300 K and increases with the decrease of temperature, reaching ~10% at a maximal applied magnetic field of ±9 T and temperature 2 K.

Such magnetoresistance change is typical for undoped MWCNT networks and generally is explained by the relative changes in conductivity caused by the effects of weak localization, which are proportional to the temperature-dependent phase relaxation time of the wave function, as well as charge carriers' interaction, proportional to the thermal coherence length of the charge carriers respectively [38]. The charge carrier transport of undoped MWCNT networks fits well to the Mott variable-range hopping (VRH) model for a disordered system (Fig. 4 a), following the formula $\sigma = \sigma_0 \exp(-(T_0/T)^{1/4})$, where σ_0 represents the conductivity of the sample at room temperature, and T_0 is the Mott's characteristic temperature which is related to the energy needed for hopping of charge carriers.

In that case, the magnetic field destroys phase coherence between different conducting paths which leads to negative magnetoresistance. Since regular hopping length decreases with increasing temperature due to the phonon scattering, the changes in negative magnetoresistance decrease too being proportional to magnetic flux through the area determined by the hopping and localization lengths [41].

In turn, the magnetoresistance of N-MWCNTs (Fig.s 3 b, c) demonstrates temperature-dependent behavior, which differs from the undoped MWCNTs. In the temperature range from 300 K down to 30 K the magnetoresistance of the N-MWCNTs is negative similar to the behavior of the undoped MWCNTs (Figs. 3 b and c, red, orange, and yellow curves). However, the maximal value of negative magnetoresistance reached at 30 K and magnetic field 9 T was -0.5% and -0.25% for N-MWCNTs synthesized using BZ:PY ratios 1:3 and 1:19 respectively, which is by ~11.5 and ~23 times lower in comparison with the magnetoresistance showed by undoped MWCNTs under the same conditions (30 K, 9 T).

Since the conductivity of the N-MWCNT samples in the temperature range from 300 K down to 30 K is following the Mott VRH model (Fig. 4 b), and the magnetoresistance of the samples is similar to that shown by the undoped MWCNTs: it is negative and decreasing with the increase of temperature (Fig. 3 b, c), it may be presumed that the mechanism of conductance in the N-MWCNT samples in the temperature range 30-300 K is similar to the undoped MWCNTs. Lower absolute values of magnetoresistance of the N-MWCNTs in comparison with the undoped MWCNTs (0.25 and 0.5% for N-MWCNTs synthesized using BZ:PY ratios 1:19 and 1:3 respectively vs 10% for undoped MWCNTs) may be related to the formation of shorter C-N bonds with the incorporated nitrogen compared to regular C-C bonds, which resulted in decreased electron hopping and localization lengths. In particular, a 0.02-0.04 Å bond shortening compared to carbon has been reported for graphitic nitrogen [19], while the formation of C-N bonds with lengths of 1.34 Å (vs 1.44 Å reported for C-C bonds in CNTs [42]), with an associated acceptor state just below Fermi level was reported for pyridinic nitrogen [43].

Similar by a tendency but lower by a magnitude effect of decrease of the absolute values of magnetoresistance upon nitrogen doping was observed for the N-MWCNTs synthesized using acetonitrile as a nitrogen source [20], where the absolute values of magnetoresistance of nitrogen-doped N-MWCNTs decreased by 50% from -4.8% to -2.4% at 1.6 K.

Presumably, such a strongly expressed difference in the magnetoresistance between the undoped MWCNTs and N-MWCNTs synthesized using BZ:PY precursor may be related to the higher concentration of pyridinic nitrogen defects in these N-MWCNTs (33% and 42% for N-MWCNTs synthesized using BZ:PY ratios 1:3 and 1:19 respectively, Table 1) in comparison with the N-MWCNTs synthesized using acetonitrile as a nitrogen source (28-30%, Table 1).

Further decrease of the temperature resulted in upturn of the magnetoresistance of N-MWCNTs synthesized using BZ:PY precursor in the temperature region from 15 K to 5 K (Figs. 3 b and c, green curves) and further complete switching of the magnetoresistance to positive at temperatures below 5 K (Figs. 3 b and c, blue curves).

Previous reports on the magnetoresistance of N-MWCNT synthesized using acetonitrile as the nitrogen source demonstrated negative magnetoresistance of the N-MWCNTs [20], and to the best of our knowledge, the effect of the temperature-dependent magnetoresistance switching from negative to positive values has not been observed previously for bare N-doped MWCNTs. In our case, the upturn of the magnetoresistance at higher magnetic fields in the temperature region from 15 K to 5 K may be related to the increase of sp^2 cluster size promoted by the formation of graphitic and pyridinic N defects in the structure of carbon [44–46], which reduces the overlap states of the electron wave functions, consequently decreasing the electron hopping probability between two states and resulting in positive magnetoresistance due to the wavefunction shrinkage being proportional to magnetic field and inversely proportional to temperature.

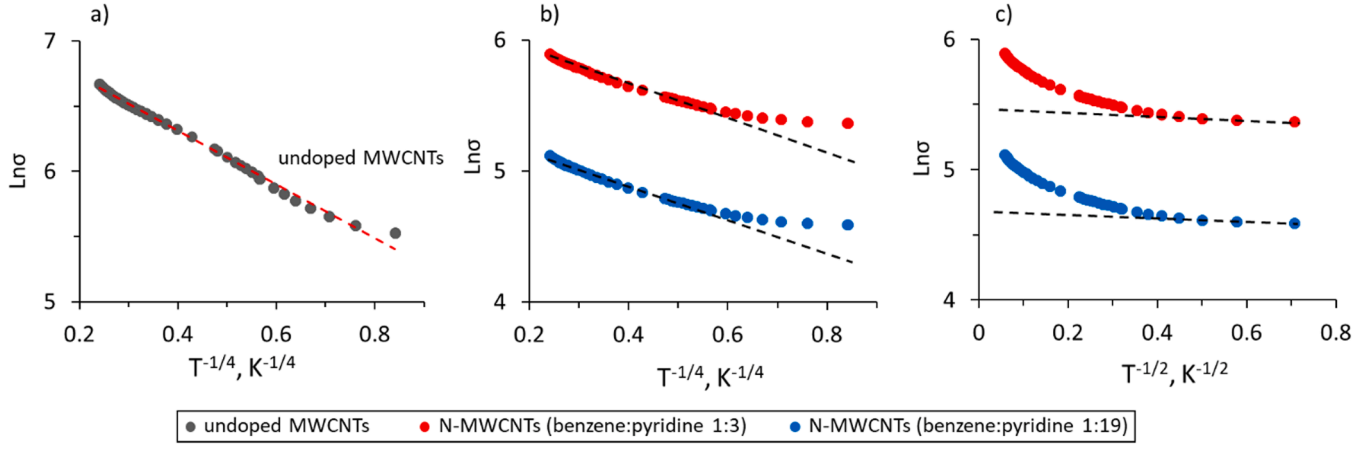

Figure 4. Temperature dependencies of conductivity of undoped MWCNTs (grey dots) and N-MWCNTs synthesized with the benzene:pyridine ratios 1:3 (red dots) and 1:19 (blue dots).

A similar effect of temperature-dependent switching of the magnetoresistance was observed previously for the graphene nanocrystallites embedded carbon film and explained in relation to nanocrystalline cluster sizes [47]. In the temperature region below 5 K and down to 2 K the magnetoresistance of N-MWCNTs became fully positive (Figs. 3 b and c, blue curves). The maximal magnetoresistance value reached by the N-MWCNTs synthesized using BZ:PY ratio 1:3 was ~2.5 higher than the value reached by the N-MWCNTs synthesized using BZ:PY ratio 1:19 (2.8% vs 1.1% respectively).

At temperatures below 5 K Mott's law is not valid (Fig. 4 b) due to the presence of Coulomb interaction between the localized electrons. At these temperatures, Efros-Shklovski (ES) model, which considers electron-electron interaction, introducing Coulomb gap at the Fermi level, was used. The ES model is described by a formula $\sigma = \sigma_0 \, exp\,(-(T_{ES}/T)^{1/2})$, where T_{ES} is the Shklovski characteristic temperature. Good fit of the conductivity of the networks of N-MWCNT synthesized using BZ:PY precursor to the ES model at temperatures below 5 K (Fig. 4 c) proves the validity of this conduction model and indicates the wave function shrinkage due to the increased number of defects in the system as dominating process, resulting in positive magnetoresistance [47]. In addition, a positive component to the total magnetoresistance of N-MWCNTs at temperatures below 5 K may be added by the spin effects in strongly localized systems, when electron spins are aligned by the external magnetic field, which results in more difficult hopping of the electrons between the energy states [48]. Lower positive magnetoresistance of the N-MWCNTs containing higher concentration of nitrogen may be related to the enlarged overlapped wave functions of localized electronic states [47] due to the higher concentration of sp^2-coordinated graphitic and pyridinic N defects (37% and 33% vs 45% and 42% for N-MWCNTs synthesized using BZ:PY ratios 1:3 and 1:19 respectively, Table 1).

3.3. Thermoelectric properties undoped MWCNTs and N-MWCNTs

Seebeck coefficient measurements of the undoped MWCNTs (Fig. 5 a, grey dots) and N-MWCNTs synthesized using BZ:PY ratios 1:3 and 1:19 (Fig. 5 a, red and blue dots respectively) were performed under high-vacuum conditions to eliminate the contribution of adsorbed oxygen to the conductance of the nanotubes.

The measurements revealed linear dependence of the Seebeck coefficient on the temperature for the N-MWCNTs, indicating that electrons are degenerate to have the Fermi energy larger than the thermal energy [49]. The Seebeck coefficient of undoped MWCNTs showed negative values, which confirms that the natural p-type conductance of undoped MWCNTs is a result of the dominating contribution of oxygen absorbed on the surfaces of MWCNTs. The Seebeck coefficient of undoped MWCNTs showed a slight increase up to 200 K followed by the saturation (Fig. 5 a, grey dots).

Measured under vacuum conditions room-temperature Seebeck coefficient values of N-MWCNTs synthesized using BZ:PY ratios 1:3 and 1:19 were -12 $\mu V \cdot K^{-1}$ and -9 $\mu V \cdot K^{-1}$. These values correspond to the values of the Seebeck coefficient measured under vacuum conditions for the N-MWCNTs synthesized using toluene/pyrazine as precursor and melamine as a nitrogen source (~ -10-12 $\mu V \cdot K^{-1}$ [10]).

A slightly lower Seebeck coefficient of the N-MWCNTs synthesized using BZ:PY ratio 1:19, measured in vacuum, in comparison with the Seebeck coefficient of N-MWCNTs synthesized using BZ:PY ratio 1:3 may be related to the higher number of pyridinic nitrogen defects (42% vs 33% for N-MWCNT synthesized using BZ:PY ratio 1:3, Table 1) with acceptor states impacting charge carrier concentration.

Calculated using the power factor (PF) of the N-MWCNTs synthesized using BZ:PY precursor showed quadratic dependencies on temperature, reaching 10 $nW \cdot m^{-1} \cdot K^{-2}$ and 60 $nW \cdot m^{-1} \cdot K^{-2}$ at room temperature for the samples synthesized using BZ:PY ratios 1:19 and 1:3 respectively (Fig. 3 b, blue and red dots), which is ~16.5 and 100 times higher than the PF shown by undoped MWCNTs measured under high-vacuum conditions (Fig. 5 b, grey dots). In addition, the undoped MWCNTs showed an increase of the PF up to 200 K, followed by saturation (Fig. 3 b, inset).

Presumably, in the case of the N-MWCNTs the main contribution to the n-type conductance is provided by graphitic N defects, generating donor states [19,50], while in the case of undoped MWCNTs the n-type conductance is the result of the competing contribution of negative and positive charge carriers. The lower total conductivity of the N-MWCNTs synthesized using BZ:PY ratio 1:19 in comparison with that of N-MWCNTs synthesized using BZ:PY ratio 1:3 (Fig. 3 a) may be explained by the higher concentration of pyridinic defects having acceptor states relative to the graphitic defects (0.93 vs 0.89 respectively, Table 1).

The absolute values of the Seebeck coefficient measured in ambient air showed a decrease of its values by ~2.4 and ~1.3 times for N-MWCNTs synthesized using BZ:PY ratios 1:3 and 1:19 respectively, resulting in Seebeck coefficient values of ~ -5 and -7 $\mu V \cdot K^{-1}$ (Table 2). In turn, undoped MWCNTs showed positive values of the Seebeck coefficient of ~ 9 $\mu V \cdot K^{-1}$ (Table 2).

The decrease of the absolute values of the Seebeck coefficient of N-MWCNTs and the change of the sign of the Seebeck coefficient of undoped MWCNTs from negative to positive may be explained by the impact of adsorbed from the environment oxygen [10,11].

These values are comparable with the Seebeck coefficient values reported for N-MWCNT powders synthesized using acetonitrile (~ -7.3 to -12.7 $\mu V \cdot K^{-1}$ [12,51]) as the nitrogen source. It should be noted that

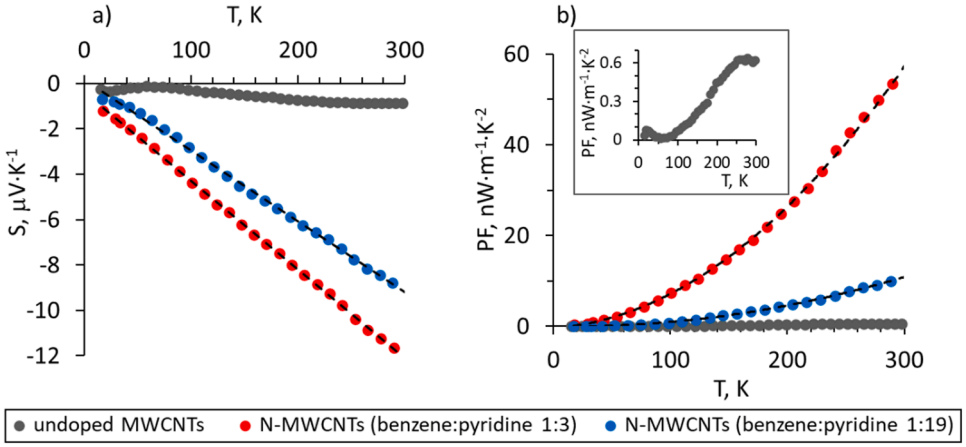

Figure 5. Seebeck coefficient (a) and power factor (b) vs temperature of undoped MWCNTs (grey dots) and N-MWCNT synthesized using BZ:PY ratios 1:3 (red dots) and 1:19 (blue dots) measured under vacuum conditions.

Table 2
Room-temperature Seebeck coefficient of N-MWCNTs measured in vacuum and in ambient air before and after annealing at 500°C in air for 40 mins.

Sample	BZ:PY ratio	S measured in vacuum, $\mu V \cdot K^{-1}$	S before annealing, $\mu V \cdot K^{-1}$	S after annealing, $\mu V \cdot K^{-1}$	S a month after annealing, $\mu V \cdot K^{-1}$
N-MWCNTs	1:3	-12 ± 2	-5 ± 1	-5.5 ± 1	-5.6 ± 0.7
	1:19	-9 ± 1	-7 ± 3	-9 ± 1.5	–
Undoped MWCNTs	–	-0.85 ± 0.05	$+9 \pm 2$	–	–

to the best of our knowledge, the stability of the Seebeck coefficient of N-MWCNTs upon annealing in air has not been previously investigated despite the importance of this issue for thermoelectrical applications.

In our work, annealing of the N-MWCNTs synthesized using BZ:PY precursor in air at 500 °C for 40 minutes showed that the values of the Seebeck coefficient of N-MWCNTs still remained negative and even showed an increase by 10 and 30% for the N-MWCNTs synthesized using BZ:PY ratios 1:3 and 1:19 respectively (Table 2).

The stability of the Seebeck coefficient during and after annealing in air indicates that the electronic changes induced by nitrogen doping overwhelm the corresponding changes caused by the absorbed on the surfaces of the N-MWCNT nanotubes oxygen.

The Seebeck coefficient values of the N-MWCNTs, measured a month after annealing for the N-MWCNTs synthesized using BZ:PY ratio 1:3 did not show a decrease in comparison with the values of the Seebeck coefficient obtained immediately after the annealing (Table 2), proving the stability of the electronic changes introduced by nitrogen doping.

Presumably, the main contributor to the n-type conductance in the N-MWCNTs is graphitic nitrogen, which in contrast to nondoping in sp^2 state pyridinic nitrogen creates a donor state at ~0.18 eV [50] and is incorporated mostly in the shells of MWCNTs, which are closer to the nanotube core and are less impacted by the adsorbed on the surface of the MWCNT nitrogen. Similar incorporation of the nitrogen in the graphitic form in the inner shells of the nanotubes was previously reported for the N-MWCNTs, synthesized using a mixture of benzene and acetonitrile [21]. Consequently, the higher concentration of graphitic N defects (45% vs 37% for N-MWCNTs synthesized using BZ:PY ratios 1:19 and 1:3 respectively) resulted in slightly higher absolute values of Seebeck coefficients measured in air (7-9 $\mu V \cdot K^{-1}$ vs 5-5.5 $\mu V \cdot K^{-1}$ for N-MWCNTs synthesized using BZ:PY ratios 1:19 and 1:3 respectively).

Annealing in the air may result in partial transformation of pyridinic and pyrrolic defects in their structure to additional graphitic defects [21,22,52], which will result in a slight increase of the Seebeck coefficient due to the increase of charge carrier concentration provided by the donor states of the additional graphitic N.

Despite the relatively low Seebeck coefficient and consequently, PF of the bare n-type N-MWCNT networks, the stability of their n-type conductivity makes them perspective for the applications in highly-efficient flexible n-type thermoelectric heterostructured networks, where inorganic n-type thermoelectric nanostructures (Bi_2Te_3, Bi_2Se_3) are directly deposited on the CNT network [4,53]. Previously, it has been reported that MWCNT-Bi_2Se_3 networks with 1.5-2 wt.% of undoped p-type MWCNTs were able to achieve Seebeck coefficient ~ -85 $\mu V \cdot K^{-1}$, however, the resistance of these networks was in order of 10^4 Ω [4]. Increase of the content of undoped MWCNTs up to ~3-4 wt.% resulted in the decrease in the resistance of MWCNT-Bi_2Se_3 heterostructured networks by an order of magnitude, however, competing conductance mechanisms of undoped MWCNTs and Bi_2Se_3 led also to the decrease of the Seebeck coefficient of the MWCNT-Bi_2Se_3 heterostructured networks by approx. factor of 2 [4]. Application of n-type N-MWCNTs may effectively solve the issue with the decrease of the Seebeck coefficient of the MWCNT-Bi_2Se_3 heterostructured networks due to the same conduction type of the network components. Comparison of the preliminary results on the Seebeck coefficient of the MWCNT-Bi_2Se_3 heterostructured networks prepared using ~ 3 wt.% N-doped MWCNTs with similar heterostructure prepared using undoped MWCNTs, as well as with the bulk Bi_2Se_3 and rigid Bi_2Se_3 nanostructured film showed that replacement of undoped MWCNTs with N-MWCNTs in the heterostructures resulted in the increase of its Seebeck coefficient by factor 2.5-3 (Table 3).

Table 3
Seebeck coefficient, resistance, and relative comparison of PF of MWCNT-Bi_2Se_3 heterostructured networks containing ~ 3 wt.% of undoped or N-doped MWCNTs.

Sample	Seebeck coefficient, $\mu V \cdot K^{-1}$
N-MWCNT (3.3 wt.%)-Bi_2Se_3, this work	-110 ± 10
Undoped MWCNT (3.1 wt.%)-Bi_2Se_3, this work	-35 ± 5
Undoped MWCNT (3 wt.%) (Bayer)-Bi_2Se_3 [4]	-45 ± 5
Bulk Bi_2Se_3 [55]	−59
Bi_2Se_3 nanostructured film on a glass substrate [4]	−110
Bi_2Se_3 nanoparticles [54]	−115

Reached by the N-MWCNT-Bi_2Se_3 heterostructures Seebeck coefficient (~ -110 $\mu V \cdot K^{-1}$) exceeded the Seebeck coefficient of bulk Bi_2Se_3 by factor of 2 (-110 $\mu V \cdot K^{-1}$ vs -59 $\mu V \cdot K^{-1}$) and was similar to the Seebeck coefficient values of Bi_2Se_3 nanostructured films (~ -110 $\mu V \cdot K^{-1}$ [4]) and sintered Bi_2Se_3 nanoparticles (~ -115 $\mu V \cdot K^{-1}$ [54]).

4. Conclusions

Nitrogen-doped MWCNTs were synthesized via spray-assisted chemical vapor deposition process using BZ:PY precursor in ratios 1:3 and 1:19. Incorporation of N in the MWCNTs in total concentration of ~ 5 at.% was proved by complementary EDX and FTIR analyses. Analysis of the morphology of the synthesized N-MWCNTs showed a typical for nitrogen-doped MWCNTs bamboo-like structure, indicating the incorporation of nitrogen in the structure of MWCNTs. The XPS study of the N-MWCNTs revealed the presence of 3 common types of nitrogen defects: graphitic, pyridinic, and pyrrolic in ratios 1.2: 1.1: 1 and 3.5: 3.2: 1 for N-MWCNTs synthesized with BZ:PY ratios 1:3 and 1:19 respectively. These results showed that the increase of the amount of nitrogen source led to the increase of concentration of sp^2-coordinated graphitic and pyridinic nitrogen defects in the nanotube, while the number of sp^3-coordinated pyrrolic defects was significantly reduced.

Measurements of temperature dependence of the magnetoresistance of the N-MWCNTs in the temperature range 2 - 300 K revealed that in contrast with undoped MWCNTs, the magnetoresistance of N-MWCNT exhibited upturn from negative to positive with the decrease of temperature below 30 K, and further full switch of the magnetoresistance to positive at temperatures below 5 K. This effect was observed for the N-MWCNTs for the first time and was attributed to the impact of sp^2-coordinated graphitic and pyridinic nitrogen defects, resulting in an increase of sp^2 clusters. This led to the reduction of overlapping of electron wave functions, and consequently, in wave function shrinkage and spin effects in strongly localized systems under high magnetic fields and low temperatures.

Pronounced temperature-dependent changes in the magnetoresistance of the N-MWCNTs and positive magnetoresistance at low temperatures make this type of N-MWCNT perspective for the application in low-temperature electronics and sensors. Study of the thermoelectrical properties of the N-MWCNTs revealed n-type conductance and Seebeck coefficient with absolute values reaching ~12 $\mu V \cdot K^{-1}$ under high vacuum conditions and ~7 $\mu V \cdot K^{-1}$ in air. The first-time investigation of the stability of the Seebeck coefficient of N-MWCNTs upon annealing in air at a temperature of 500 °C revealed that the Seebeck coefficient remains

negative and even shows a slight increase. Such remarkable environmental stability of the n-type N-MWCNTs synthesized using BZ:PY precursor makes this material attractive for flexible thermoelectric applications, for example, for the use as the substrate for the deposition of n-type nanostructured inorganic thermoelectric materials to obtain flexible n-type N-MWCNT-TE heterostructures with Seebeck coefficient, comparable or exceeding the Seebeck coefficient values of rigid inorganic counterparts as bulk material or nanostructured films deposited on solid substrates.

Funding

This work was funded by the European Regional Development Fund (ERDF) project no. 1.1.1.1/19/A/138. A.S. and K. S. acknowledge the funding from the European Union's Horizon 2020 Framework Programme H2020-WIDESPREAD-01-2016-2017-Teaming Phase2 under grant agreement No. 739508, project CAMART^2.

Declaration of Competing Interest

The authors declare that they have no known competing financial interests or personal relationships that could have appeared to influence the work reported in this paper.

Data availability

Data will be made available on request.

Acknowledgments

The Authors acknowledge Dr. Arturs Zarins and Ms. Liga Avotina for their assistance with the FTIR measurements and analysis.

References

[1] K.S. Ibrahim, Carbon nanotubes-properties and applications: a review, Carbon Lett 14 (2013) 131–144, https://doi.org/10.5714/cl.2013.14.3.131.
[2] C.A. Hewitt, D.L. Carroll, Carbon nanotube-based polymer composite thermoelectric generators, ACS Symp. Ser. 1161 (2014) 191–211, https://doi.org/10.1021/bk-2014-1161.ch009.
[3] X. Wang, H. Wang, B. Liu, Carbon nanotube-based organic thermoelectric materials for energy harvesting, Polymers (Basel) 10 (2018), https://doi.org/10.3390/polym10111196.
[4] K. Buks, J. Andzane, K. Smits, J. Zicans, J. Bitenieks, A. Zarins, D. Erts, Growth mechanisms and related thermoelectric properties of innovative hybrid networks fabricated by direct deposition of Bi2Se3 and Sb2Te3 on multiwalled carbon nanotubes, Mater. Today Energy. 18 (2020), 100526, https://doi.org/10.1016/j.mtener.2020.100526.
[5] J. Bitenieks, K. Buks, R. Merijs-Meri, J. Andzane, T. Ivanova, L. Bugovecka, V. Voikiva, J. Zicans, D. Erts, Flexible N-Type Thermoelectric Composites Based on Non-Conductive Polymer with Innovative Bi_2Se_3-CNT Hybrid Nanostructured Filler, Polymers (Basel) 13 (2021) 4264, https://doi.org/10.3390/polym13234264.
[6] K. Buks, J. Andzane, L. Bugovecka, M.V Katkov, K. Smits, O. Starkova, J. Katkevics, A. Bērziņš, L. Brauna, V. Voikiva, D. Erts, Highly Efficient Flexible n-Type Thermoelectric Films Formed by Encapsulation of Bi_2Se_3-MWCNT Hybrid Networks in Polyvinyl Alcohol, Adv. Mater. Interfaces (2022), 2200318, https://doi.org/10.1002/admi.202200318.
[7] J. Andzane, K. Buks, J. Bitenieks, L. Bugovecka, A. Kons, R. Merijs-meri, J. Svirksts, J. Zicans, D. Erts, p-Type PVA/MWCNT-Sb_2Te_3 Composites for Application in Different Types of Flexible Thermoelectric Generators in Combination with n-Type PVA/MWCNT-Bi_2Se_3 Composites, Polymers 14 (2022) 5130, https://doi.org/10.3390/polym14235130.
[8] L. Brownlie, J. Shapter, Advances in carbon nanotube n-type doping: Methods, analysis and applications, Carbon N. Y. 126 (2018) 257–270, https://doi.org/10.1016/j.carbon.2017.09.107.
[9] H.Y. Miao, J.H. Liu, L. Saravanan, M.C. Lu, L.C. Wang, Plasma functionalization and effect of annealing on electrical properties of MWCNT buckypaper, IEEE Nanotechnol. Mater. Devices Conf. IEEE NMDC (2013) 39–41, https://doi.org/10.1109/NMDC.2013.6707450, 2013.
[10] B. Sadanadan, T. Savage, S. Bhattacharya, T. Tritt, A. Cassell, M. Meyyappan, Z. R. Dai, Z.L. Wang, R. Zidan, A.M. Rao, Synthesis and thermoelectric power of nitrogen-doped carbon nanotubes, J. Nanosci. Nanotechnol. 3 (2003) 99–103, https://doi.org/10.1166/jnn.2003.186.
[11] A. Zettl, Extreme oxygen sensitivity of electronic properties of carbon nanotubes, Science 287 (2000) 1801–1804, https://doi.org/10.1126/science.287.5459.1801, 80-.
[12] B. Krause, I. Konidakis, M. Arjmand, U. Sundararaj, R. Fuge, M. Liebscher, S. Hampel, M. Klaus, E. Serpetzoglou, E. Stratakis, P. Pötschke, Nitrogen-doped carbon nanotube/polypropylene composites with negative seebeck coefficient, J. Compos. Sci. 4 (2020) 14, https://doi.org/10.3390/jcs4010014.
[13] B. Kumanek, G. Stando, P.S. Wróbel, M. Krzywiecki, D. Janas, Thermoelectric properties of composite films from multi-walled carbon nanotubes and ethyl cellulose doped with heteroatoms, Synth. Met. 257 (2019), 116190, https://doi.org/10.1016/j.synthmet.2019.116190.
[14] I. Kunadian, R. Andrews, M. Pinar Mengüç, D. Qian, Thermoelectric power generation using doped MWCNTs, Carbon N. Y. 47 (2009) 589–601, https://doi.org/10.1016/j.carbon.2008.10.043.
[15] M. Kumar, Y. Ando, Chemical vapor deposition of carbon nanotubes: A review on growth mechanism and mass production, J. Nanosci. Nanotechnol. 10 (2010) 3739–3758, https://doi.org/10.1166/jnn.2010.2939.
[16] S.S. Meysami, F. Dillon, A.A. Koós, Z. Aslam, N. Grobert, Aerosol-assisted chemical vapour deposition synthesis of multi-wall carbon nanotubes: I. Mapping the reactor, Carbon N. Y. 58 (2013) 151–158, https://doi.org/10.1016/j.carbon.2013.02.041.
[17] R.A. Ismail, M.H. Mohsin, A.K. Ali, K.I. Hassoon, S. Erten-Ela, Preparation and characterization of carbon nanotubes by pulsed laser ablation in water for optoelectronic application, Phys. E Low-Dimensional Syst. Nanostructures. 119 (2020), 113997, https://doi.org/10.1016/j.physe.2020.113997.
[18] Z. Li, J. Andzane, D. Erts, J.M. Tobin, K. Wang, M.A. Morris, G. Attard, J. D. Holmes, A supercritical-fluid method for growing carbon nanotubes, Adv. Mater. 19 (2007) 3043–3046, https://doi.org/10.1002/adma.200602483.
[19] C.P. Ewels, M. Glerup, Nitrogen doping in carbon nanotubes, J. Nanosci. Nanotechnol. 5 (2005) 1345–1363, https://doi.org/10.1166/jnn.2005.304.
[20] I.V. Ovsienko, T.A. Len, L.Y. Matsuy, Y.I. Prylutskyy, I.B. Berkutov, V. V. Andrievskii, Y.F. Komnik, I.G. Mirzoiev, G.E. Grechnev, Y.A. Kolesnichenko, R. Hayn, P. Scharff, Magnetoresistance and electrical resistivity of N-doped multi-walled carbon nanotubes at low temperatures, Phys. Status Solidi Basic Res. 252 (2015) 1402–1409, https://doi.org/10.1002/pssb.201451657.
[21] L.G. Bulusheva, A.V. Okotrub, Y.V. Fedoseeva, A.G. Kurenya, I.P. Asanov, O. Y. Vilkov, A.A. Koós, N. Grobert, Controlling pyridinic, pyrrolic, graphitic, and molecular nitrogen in multi-wall carbon nanotubes using precursors with different N/C ratios in aerosol assisted chemical vapor deposition, Phys. Chem. Chem. Phys. 17 (2015) 23741–23747, https://doi.org/10.1039/c5cp01981h.
[22] H. Liu, Y. Zhang, R. Li, X. Sun, H. Abou-Rachid, Thermal and chemical durability of nitrogen-doped carbon nanotubes, J. Nanoparticle Res. 14 (2012) 1016, https://doi.org/10.1007/s11051-012-1016-0.
[23] T. Sharifi, F. Nitze, H.R. Barzegar, C.W. Tai, M. Mazurkiewicz, A. Malolepszy, L. Stobinski, T. Wågberg, Nitrogen doped multi walled carbon nanotubes produced by CVD-correlating XPS and Raman spectroscopy for the study of nitrogen inclusion, Carbon N. Y. 50 (2012) 3535–3541, https://doi.org/10.1016/j.carbon.2012.03.022.
[24] P. Nemes-Incze, N. Daróczi, Z. Sárközi, A.A. Koós, K. Kertész, O. Ţiprigan, Z. E. Horváth, A.L. Darabont, L.P. Biró, Synthesis of bamboo - Structured multiwalled carbon nanotubes by spray pyrolysis method, using a mixture of benzene and pyridine, J. Optoelectron. Adv. Mater. 9 (2007) 1525–1529.
[25] R. Sen, B.C. Satishkumar, A. Govindaraj, K.R. Harikumar, G. Raina, J.P. Zhang, A. K. Cheetham, C.N.R. Rao, B-C-N, C-N and B-N nanotubes produced by the pyrolysis of precursor molecules over Co catalysts, Chem. Phys. Lett. 287 (1998) 671–676, https://doi.org/10.1016/S0009-2614(98)00220-6.
[26] Y. Togashi, T. Hatori, Y. Nakamura, N. Aoki, J.P. Bird, M. Terrones, K. Kanako, Y. Ochiai, Magnetoresistance and phase breaking behavior of a nitrogen doped multi-walled carbon nanotube, Jpn. J. Appl. Phys. 49 (2010) 02BD01, https://doi.org/10.1143/JJAP.49.02BD01.
[27] R. Zhang, W. Lv, G. Li, L. Lei, Electrochemical reduction of CO2 on SnO2/nitrogen-doped multiwalled carbon nanotubes composites in KHCO3 aqueous solution, Mater. Lett. 141 (2015) 63–66, https://doi.org/10.1016/j.matlet.2014.11.040.
[28] S. Boncel, S.W. Pattinson, V. Geiser, M.S.P. Shaffer, K.K.K. Koziol, En route to controlled catalytic CVD synthesis of densely packed and vertically aligned nitrogen-doped carbon nanotube arrays, Beilstein J. Nanotechnol. 5 (2014) 219–233, https://doi.org/10.3762/bjnano.5.24.
[29] A. Misra, P.K. Tyagi, P. Rai, D.S. Misra, FTIR spectroscopy of multiwalled carbon nanotubes: A simple approach to study the nitrogen doping, J. Nanosci. Nanotechnol. 7 (2007) 1820–1823, https://doi.org/10.1166/jnn.2007.723.
[30] M. Mastalerz, R.M. Bustin, Application of reflectance micro-Fourier transform infrared spectrometry in studying coal macerals: comparison with other Fourier transform infrared techniques, Fuel 74 (1995) 536–542, https://doi.org/10.1016/0016-2361(95)98356-J.
[31] L. Avotina, E. Pajuste, M. Romanova, A. Zaslavskis, G. Enichek, V. Kinerte, A. Zarins, B. Lescinskis, J. Dehtjars, G. Kizane, Ftir analysis of electron irradiated single and multilayer Si_3N_4 coatings, Key Eng. Mater. 788 (2018) 96–101, https://doi.org/10.4028/www.scientific.net/KEM.788.96.
[32] E.N. Nxumalo, N.J. Coville, Nitrogen doped carbon nanotubes from organometallic compounds: A review, Materials (Basel) 3 (2010) 2141–2171, https://doi.org/10.3390/ma3032141.
[33] P. Szroeder, N.G. Tsierkezos, P. Scharff, U. Ritter, Electrocatalytic properties of carbon nanotube carpets grown on Si-wafers, Carbon N. Y. 48 (2010) 4489–4496, https://doi.org/10.1016/j.carbon.2010.08.009.
[34] A. Hachimi, B. Merzougui, A. Hakeem, T. Laoui, G.M. Swain, Q. Chang, M. Shao, M.A. Atieh, Synthesis of Nitrogen-doped carbon nanotubes using injection-vertical

chemical vapor deposition: Effects of synthesis parameters on the nitrogen content, J. Nanomater. (2015) 14–22, https://doi.org/10.1155/2015/453725, 2015.
[35] X. Wu, Y. Tao, Y. Lu, L. Dong, Z. Hu, High-pressure pyrolysis of melamine route to nitrogen-doped conical hollow and bamboo-like carbon nanotubes, Diam. Relat. Mater. 15 (2006) 164–170, https://doi.org/10.1016/j.diamond.2005.09.018.
[36] S. Point, T. Minea, B. Bouchet-Fabre, A. Granier, G. Turban, XPS and NEXAFS characterisation of plasma deposited vertically aligned N-doped MWCNT, Diam. Relat. Mater. 14 (2005) 891–895, https://doi.org/10.1016/j.diamond.2004.10.011.
[37] U. Ritter, N.G. Tsierkezos, Y.I. Prylutskyy, L.Y. Matzui, V.O. Gubanov, M.M. Bilyi, M.O. Davydenko, Structure-electrical resistivity relationship of N-doped multi-walled carbon nanotubes, J. Mater. Sci. 47 (2012) 2390–2395, https://doi.org/10.1007/s10853-011-6059-6.
[38] I.V. Ovsiienko, T.A. Len, I.G. Mirzoiev, E.Y. Beliayev, D. Gnida, L.Y. Matzui, V. M. Heraskevych, Low-temperature magnetoresistance of multi-walled carbon nanotubes with perfect structure, Low Temp. Phys. 48 (2022) 89–98, https://doi.org/10.1063/10.0009286.
[39] T. Abraham, C. Bansal, Logarithmic temperature dependence of conductivity in a random quasi-two dimensional assembly of gold nanoclusters, J. Phys. Commun. 1 (2017), 015008, https://doi.org/10.1088/2399-6528/aa81b6.
[40] K.B. Efetov, A. Tschersich, Coulomb effects in granular materials at not very low temperatures, Phys. Rev. B - Condens. Matter Mater. Phys. 67 (2003), 174205, https://doi.org/10.1103/PhysRevB.67.174205.
[41] G. Baumgartner, M. Carrard, L. Zuppiroli, W. Bacsa, W.A. de Heer, L. Forró, Hall effect and magnetoresistance of carbon nanotube films, Phys. Rev. B - Condens. Matter Mater. Phys. 55 (1997) 6704–6707, https://doi.org/10.1103/PhysRevB.55.6704.
[42] A. Aqel, K.M.M.A. El-Nour, R.A.A. Ammar, A. Al-Warthan, Carbon nanotubes, science and technology part (I) structure, synthesis and characterisation, Arab. J. Chem. 5 (2012) 1–23, https://doi.org/10.1016/j.arabjc.2010.08.022.
[43] M. Zhao, Y. Xia, J.P. Lewis, R. Zhang, First-principles calculations for nitrogen-containing single-walled carbon nanotubes, J. Appl. Phys. 94 (2003) 2398–2402, https://doi.org/10.1063/1.1593798.
[44] M.V. Katkov, R. McIntosh, S. Bhattacharyya, Tunnel transport model in nitrogen doped disordered carbon superstructures, J. Appl. Phys. 113 (2013), 093701, https://doi.org/10.1063/1.4794020.
[45] J. Robertsona, C.A. Davisb, EiAMOND RELATED MATERIALS Nitrogen doping of tetrahedral amorphous carbon, Diam. Relat. Mater. 4 (1995) 44–444.
[46] S.E. Rodil, W.I. Milne, J. Robertson, L.M. Brown, Maximized sp^3 bonding in carbon nitride phases, Appl. Phys. Lett. 77 (2000) 1458–1460, https://doi.org/10.1063/1.1308273.
[47] D. Ding, X. Dai, C. Wang, D. Diao, Temperature dependent crossover between positive and negative magnetoresistance in graphene nanocrystallines embedded carbon film, Carbon N. Y. 163 (2020) 19–25, https://doi.org/10.1016/j.carbon.2020.03.022.
[48] A. Kurobe, H. Kamimura, Correlation Effects on Variable Range Hopping Conduction and the Magnetoresistance, JPSJ 51 (1982) 1904–1913.
[49] I. Terasaki, Thermal Conductivity and Thermoelectric Power of Semiconductors, Compr. Semicond. Sci. Technol. 1–6 (2011) 326–358, https://doi.org/10.1016/B978-0-44-453153-7.00070-5.
[50] R. Czerw, M. Terrones, J.C. Charlier, X. Blase, B. Foley, R. Kamalakaran, N. Grobert, H. Terrones, D. Tekleab, P.M. Ajayan, W. Blau, M. Rühle, D.L. Carroll, Identification of Electron Donor States in N-Doped Carbon Nanotubes, Nano Lett 1 (2001) 457–460, https://doi.org/10.1021/nl015549q.
[51] B. Krause, C. Barbier, J. Levente, M. Klaus, P. Pötschke, Screening of different carbon nanotubes in melt-mixed polymer composites with different polymer matrices for their thermoelectrical properties, J. Compos. Sci. 3 (2019) 106, https://doi.org/10.3390/jcs3040106.
[52] S.C. Ray, Nitrogenated Carbon Nanotubes Functionalized with Chlorine and Oxygen: Electronic and magnetic properties for electronic/magnetic device applications, Front. Res. Today. 1 (2018) 1006, https://doi.org/10.31716/frt.201801006.
[53] Q. Jin, S. Jiang, Y. Zhao, D. Wang, J. Qiu, D.M. Tang, J. Tan, D.M. Sun, P.X. Hou, X. Q. Chen, K. Tai, N. Gao, C. Liu, H.M. Cheng, X. Jiang, Flexible layer-structured Bi_2Te_3 thermoelectric on a carbon nanotube scaffold, Nat. Mater. 18 (2019) 62–68, https://doi.org/10.1038/s41563-018-0217-z.
[54] K. Kadel, L. Kumari, W.Z. Li, J.Y. Huang, P.P. Provencio, Synthesis and Thermoelectric Properties of Bi_2Se_3 Nanostructures, Nanoscale Res. Lett. 6 (2011) 57, https://doi.org/10.1007/s11671-010-9795-7.
[55] J. Navrátil, J. Horák, T. Plecháček, S. Kamba, P. Lošťák, J.S. Dyck, W. Chen, C. Uher, Conduction band splitting and transport properties of Bi_2Se_3, J. Solid State Chem. 177 (2004) 1704–1712, https://doi.org/10.1016/j.jssc.2003.12.031.